Journal of Zhejiang University-SCIENCE C (Computers & Electronics)
ISSN 1869-1951 (Print); ISSN 1869-196X (Online)
www.zju.edu.cn/jzus; www.springerlink.com
E-mail: jzus@zju.edu.cn

Underwater glider design based on dynamic model analysis and prototype development*

Shuang-shuang FAN†, Can-jun YANG†‡, Shi-lin PENG, Kai-hu LI, Yu XIE, Shao-yong ZHANG

(*The State Key Lab of Fluid Power Transmission and Control, Zhejiang University, Hangzhou 310027, China*)

†E-mail: fanshuangshuang@163.com; ycj@zju.edu.cn

Received Jan. 2, 2013; Revision accepted Apr. 11, 2013; Crosschecked July 12, 2013

Abstract: Underwater gliders are efficient mobile sensor platforms that can be deployed for months at a time, traveling thousands of kilometers. Here, we describe our development of a coastal 200 m deep underwater glider, which can serve as an ocean observatory platform operating in the East China Sea. Our glider is developed based on dynamic model analysis: steady flight equilibrium analysis gives the varied range of moving mass location for pitch control and the varied vehicle volume for buoyancy control; a stability analysis is made to discuss the relationship between the stability of glider motion and the location of glider wings and rudder by root locus investigation of glider longitudinal- and lateral-directional dynamics, respectively. There is a tradeoff between glider motion stability and control authority according to the specific glider mission requirements. The theoretical analysis provides guidelines for vehicle design, based on which we present the development progress of the Zhejiang University (ZJU) glider. The mechanical, electrical, and software design of the glider is discussed in detail. The performances of glider key functional modules are validated by pressure tests individually; preliminary pool trials of the ZJU glider are also introduced, indicating that our glider functions well in water and can serve as a sensor platform for ocean sampling.

Key words: Underwater glider design, Equilibrium, Stability, Pressure test, Pool trial
doi:10.1631/jzus.C1300001 **Document code:** A **CLC number:** TP242

1 Introduction

An underwater glider is a type of autonomous underwater vehicle (AUV) that uses buoyancy control and lifting surfaces to propel itself forward following an up-and-down, sawtooth-like profile through the water, with very low power consumption. Since first envisioned by Stommel (1989), underwater gliders have received increasing attention worldwide and have transitioned from a concept to a technology serving as an appealing sensor platform for ocean observatory (Rudnick *et al.*, 2004). It can be deployed for months at a time, traveling thousands of kilometers. Efforts have focused on the development of underwater glider for decades. Nowadays, there are several types of underwater gliders applied for ocean sampling, such as the three legendary gliders: Slocum (Webb *et al.*, 2001), Seaglider (Eriksen *et al.*, 2001), and Spray (Sherman *et al.*, 2001). As the underwater glider becomes a technology undergoing active and rapid development, much theoretical analysis work has been carried out on glider dynamics (Graver, 2005; Wang *et al.*, 2011), performance, and stability analysis (Jenkins *et al.*, 2003; Yu *et al.*, 2011) as well as motion control (Leonard and Graver, 2001; Li *et al.*, 2008; Mahmoudian and Woolsey, 2008; Yang and Ma, 2010; Hussain *et al.*, 2011) and path planning (Mahmoudian *et al.*, 2010) based on the glider dynamic model. However, glider development and theoretical research are separate to some extent in the previous work. There is less systematic theoretical analysis providing guidelines for glider development, which is based on dynamic model analysis to obtain the basic design parameters.

‡ Corresponding author

* Project supported by the National Natural Science Foundation of China (No. 51221004) and the Natural Science Foundation of Zhejiang Province, China (No. R1090453)

Here, we describe our development of a coastal 200 m depth underwater glider, which can serve as an ocean observatory platform operating in the East China Sea. Our glider is developed based on dynamic model analysis: steady flight equilibrium analysis gives the varied range of moving mass location for pitch control and vehicle volume for buoyancy control; a stability analysis is made to discuss the relationship between the stability of glider motion and the location of glider wings and rudder by root locus investigation of glider longitudinal- and lateral-directional dynamics, respectively. There is a tradeoff between glider motion stability and control authority according to the specific glider mission requirements. Theoretical analysis provides guidelines for vehicle design, based on which we present the development progress of the ZJU glider in detail.

2 Dynamic model

The multi-body glider is modeled as a rigid body (mass m_{rb}) with a single moving point mass m_{p}, which can move longitudinally along the vehicle's centerline. The vehicle also includes a variable ballast actuator whose effect is represented by a fixed-position point mass m_{b} with variable volume $\tilde{V}_{\mathrm{b}}$. The total vehicle mass is

$$m = m_{\mathrm{rb}} + m_{\mathrm{p}} + m_{\mathrm{b}}.$$

The vehicle displaces a deformable volume of fluid V_{veh} so that the net weight can be described as

$$W = mg - \rho g V_{\mathrm{veh}} = -\rho g \tilde{V}_{\mathrm{b}},$$

where the rate of change of varied volume $\tilde{V}_{\mathrm{b}}$ is an input, enabling buoyancy-powered propulsion. Note that we have defined a deformable control volume around the vehicle, so that the vehicle's buoyancy varies, with its mass fixed. Alternatively, one could define a deformable control mass, in which case buoyancy would remain constant and the vehicle mass would vary. If W is greater than zero, the vehicle is heavier than the fluid it displaces and tends to sink, while if W is negative, the vehicle is buoyant and tends to rise.

The multi-body glider has eight degrees of freedom. Except for the conventional six degrees of rigid body (translational motions: surging, swaying, heaving; rotational motions: pitching, rolling, yawing), a longitudinal moving particle for pitch control and a rudder for directional control add the other two degrees of freedom. A rudder for directional control can provide better maneuverability for a turning motion when the glider moves in shallow water.

2.1 Kinematics

Define a body-fixed, orthonormal reference frame centered at the center of buoyancy of the vehicle and represented by the unit vectors $\boldsymbol{b}_1$, $\boldsymbol{b}_2$, and $\boldsymbol{b}_3$. The vector $\boldsymbol{b}_1$ is aligned with the longitudinal axis of the vehicle, $\boldsymbol{b}_2$ points out the right wing, and $\boldsymbol{b}_3$ completes the right-handed triad (Fig. 1). Define another orthonormal reference frame, denoted by the unit vectors $\boldsymbol{i}_1$, $\boldsymbol{i}_2$, and $\boldsymbol{i}_3$, which is fixed in inertial space such that $\boldsymbol{i}_3$ is aligned with the force due to gravity. The choices of frames are consistent with the underwater vehicle literature (Fossen, 1995). The relative orientation of these two reference frames is given by the proper rotation matrix $\boldsymbol{R}_{\mathrm{IB}}$, which maps free vectors from the body-fixed reference frame into the inertial reference frame (Fossen, 1995). Let $\boldsymbol{e}_i$ (i=1, 2, 3) represent the standard basis vectors in the 3D space, and let the character '$\hat{\ }$' denote the 3×3 skew-symmetric matrix satisfying $\hat{\boldsymbol{a}}\boldsymbol{b} = \boldsymbol{a} \times \boldsymbol{b}$ for vectors $\boldsymbol{a}$ and $\boldsymbol{b}$. Then, in terms of conventional Euler angles (roll angle φ, pitch angle θ, and heading angle ψ), we have

$$\boldsymbol{R}_{\mathrm{IB}}(\varphi,\theta,\psi) = \mathrm{e}^{\hat{\boldsymbol{e}}_3\psi}\mathrm{e}^{\hat{\boldsymbol{e}}_2\theta}\mathrm{e}^{\hat{\boldsymbol{e}}_1\varphi},$$

where $\mathrm{e}^{(\cdot)}$ denotes the matrix exponential (Mahmoudian, 2009).

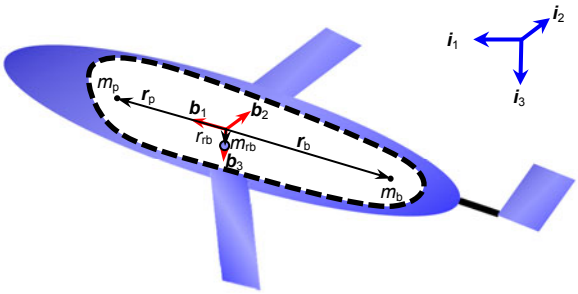

Fig. 1 Illustration of the underwater glider rigid body and mass particles

Let the inertial vector $\boldsymbol{X}=[X, Y, Z]^{\mathrm{T}}$ represent the position vector from the origin of the inertial frame to the origin of the body frame. Let $\boldsymbol{v}=[u, v, w]^{\mathrm{T}}$ and $\boldsymbol{\omega}=[p, q, r]^{\mathrm{T}}$ represent the translational and rotational velocities of the body with respect to the inertial frame, respectively, but expressed in the body frame. The kinematic equations are

$$\dot{\boldsymbol{X}}=\boldsymbol{R}_{\mathrm{IB}}\boldsymbol{v}, \tag{1}$$

$$\dot{\boldsymbol{R}}_{\mathrm{IB}}=\boldsymbol{R}_{\mathrm{IB}}\hat{\boldsymbol{\omega}}. \tag{2}$$

In addition to the six degrees of freedom associated with the vehicle's translation and rotation, there is one degree of freedom associated with the moving mass, which is modeled as a particle moving along $\boldsymbol{b}_1$ and used for pitch angle regulation. Let $\boldsymbol{r}_{\mathrm{p}}=[r_{p_x}, 0, 0]^{\mathrm{T}}$ denote the particle position with respect to the body frame origin, expressed in the body frame. The kinematics of the moving mass particle relative to the inertial space is

$$\boldsymbol{v}_{\mathrm{p}}=\boldsymbol{v}+\boldsymbol{\omega}\times\boldsymbol{r}_{\mathrm{p}}+\dot{r}_{p_x}\boldsymbol{b}_1. \tag{3}$$

Note that we may also write

$$\boldsymbol{v}_{\mathrm{p}}=[\boldsymbol{I},\ -\hat{\boldsymbol{r}}_{\mathrm{p}},\ \boldsymbol{e}_1]\boldsymbol{\eta},$$

where $\boldsymbol{\eta}=[\boldsymbol{v}^{\mathrm{T}},\ \boldsymbol{\omega}^{\mathrm{T}},\ \dot{r}_{p_x}]^{\mathrm{T}}$, $\boldsymbol{I}$ is the 3×3 unit matrix, and $\boldsymbol{e}_1=[1, 0, 0]^{\mathrm{T}}$.

2.2 Dynamics

To derive the equations of motion, we must first determine the kinetic energy of the body/fluid/particle system in order to compute the momenta (Woolsey, 2005). We start by defining the energy of the particle:

$$T_{\mathrm{p}}=\frac{1}{2}m_{\mathrm{p}}\boldsymbol{v}_{\mathrm{p}}^{\mathrm{T}}\boldsymbol{v}_{\mathrm{p}}=\frac{1}{2}\boldsymbol{\eta}^{\mathrm{T}}\mathbb{M}_{\mathrm{p}}(\boldsymbol{r}_{\mathrm{p}})\boldsymbol{\eta},$$

where

$$\mathbb{M}_{\mathrm{p}}(\boldsymbol{r}_{\mathrm{p}})=m_{\mathrm{p}}\begin{pmatrix}\boldsymbol{I}\\ \hat{\boldsymbol{r}}_{\mathrm{p}}\\ \boldsymbol{e}_1^{\mathrm{T}}\end{pmatrix}\begin{pmatrix}\boldsymbol{I}\\ \hat{\boldsymbol{r}}_{\mathrm{p}}\\ \boldsymbol{e}_1^{\mathrm{T}}\end{pmatrix}^{\mathrm{T}}=\begin{pmatrix}m_{\mathrm{p}}\boldsymbol{I} & -m_{\mathrm{p}}\hat{\boldsymbol{r}}_{\mathrm{p}} & m_{\mathrm{p}}\boldsymbol{e}_1\\ m_{\mathrm{p}}\hat{\boldsymbol{r}}_{\mathrm{p}} & -m_{\mathrm{p}}\hat{\boldsymbol{r}}_{\mathrm{p}}\hat{\boldsymbol{r}}_{\mathrm{p}} & m_{\mathrm{p}}\hat{\boldsymbol{r}}_{\mathrm{p}}\boldsymbol{e}_1\\ m_{\mathrm{p}}\boldsymbol{e}_1^{\mathrm{T}} & -m_{\mathrm{p}}\boldsymbol{e}_1^{\mathrm{T}}\hat{\boldsymbol{r}}_{\mathrm{p}} & m_{\mathrm{p}}\end{pmatrix}$$

denotes the generalized inertia matrix for the moving particle.

The buoyancy control system of the glider is considered as a mass and position-fixed particle. The generalized inertia matrix for the buoyancy control system is

$$\mathbb{M}_{\mathrm{b}}=\begin{pmatrix}m_{\mathrm{b}}\boldsymbol{I} & -m_{\mathrm{b}}\hat{\boldsymbol{r}}_{\mathrm{b}} & \boldsymbol{0}\\ m_{\mathrm{b}}\hat{\boldsymbol{r}}_{\mathrm{b}} & -m_{\mathrm{b}}\hat{\boldsymbol{r}}_{\mathrm{b}}\hat{\boldsymbol{r}}_{\mathrm{b}} & \boldsymbol{0}\\ \boldsymbol{0} & \boldsymbol{0} & 0\end{pmatrix},$$

where $\boldsymbol{r}_{\mathrm{b}}=[r_{\mathrm{b}}, 0, 0]^{\mathrm{T}}$ denotes the location of the buoyancy control system with respect to the body frame origin, expressed in the body frame. Throughout the text, $\boldsymbol{0}$ represents a matrix or vector of zeros (whose dimension is clear from the context). The kinetic energy of the buoyancy control system is

$$T_{\mathrm{b}}=\frac{1}{2}\boldsymbol{\eta}^{\mathrm{T}}\mathbb{M}_{\mathrm{b}}\boldsymbol{\eta}.$$

If $\boldsymbol{J}_{\mathrm{rb}}$ denotes the 3×3 matrix of moments and products of inertia for the rigid body (Fossen, 1995), then the generalized mass matrix for the rigid body portion of the glider is

$$\mathbb{M}_{\mathrm{rb}}=\begin{pmatrix}m_{\mathrm{rb}}\boldsymbol{I} & -m_{\mathrm{rb}}\hat{\boldsymbol{r}}_{\mathrm{rb}} & \boldsymbol{0}\\ m_{\mathrm{rb}}\hat{\boldsymbol{r}}_{\mathrm{rb}} & \boldsymbol{J}_{\mathrm{rb}} & \boldsymbol{0}\\ \boldsymbol{0} & \boldsymbol{0} & 0\end{pmatrix},$$

where $\boldsymbol{r}_{\mathrm{rb}}=[0, 0, r_{\mathrm{rb}}]^{\mathrm{T}}$ denotes the center of mass position of glider rigid body portion with respect to the body frame origin, expressed in the body frame. The kinetic energy of the rigid body portion is

$$T_{\mathrm{rb}}=\frac{1}{2}\boldsymbol{\eta}^{\mathrm{T}}\mathbb{M}_{\mathrm{rb}}\boldsymbol{\eta}.$$

We finally define the generalized added inertia matrix, which accounts for the energy necessary to accelerate the fluid around the vehicle as it moves:

$$\mathbb{M}_{\mathrm{f}}=\begin{pmatrix}\boldsymbol{M}_{\mathrm{f}} & \boldsymbol{C}_{\mathrm{f}}^{\mathrm{T}} & \boldsymbol{0}\\ \boldsymbol{C}_{\mathrm{f}} & \boldsymbol{J}_{\mathrm{f}} & \boldsymbol{0}\\ \boldsymbol{0} & \boldsymbol{0} & 0\end{pmatrix},$$

where the component submatrices $\boldsymbol{M}_{\mathrm{f}}$, $\boldsymbol{J}_{\mathrm{f}}$, and $\boldsymbol{C}_{\mathrm{f}}$ represent added mass, added inertia, and hydrodynamic

coupling between the translational and rotational motions of the rigid body, respectively (Newman, 1977; Fossen, 1995). The kinetic energy of the fluid is

$$T_{\mathrm{f}}=\frac{1}{2}\boldsymbol{\eta}^{\mathrm{T}}\mathbb{M}_{\mathrm{f}}\boldsymbol{\eta}.$$

The total kinetic energy of the rigid body/fluid/particle system is

$$T=T_{\mathrm{p}}+T_{\mathrm{b}}+T_{\mathrm{rb}}+T_{\mathrm{f}}=\frac{1}{2}\boldsymbol{\eta}^{\mathrm{T}}\mathbb{M}(\boldsymbol{r}_{\mathrm{p}})\boldsymbol{\eta},$$

where $\mathbb{M}(\boldsymbol{r}_{\mathrm{p}})=\mathbb{M}_{\mathrm{p}}(\boldsymbol{r}_{\mathrm{p}})+\mathbb{M}_{\mathrm{b}}+\mathbb{M}_{\mathrm{rb}}+\mathbb{M}_{\mathrm{f}}$.

The generalized momentum is

$$\begin{pmatrix}\boldsymbol{p}\\ \boldsymbol{h}\\ p_{p_x}\end{pmatrix}=\frac{\partial T}{\partial\boldsymbol{\eta}},$$

where $\boldsymbol{p}$ is the total body translational momentum, and $\boldsymbol{h}$ is the total body angular momentum. p_{p_x} appears in the point mass momentum

$$\boldsymbol{p}_{\mathrm{p}}=\begin{pmatrix}p_{p_x}\\ p_{p_y}\\ p_{p_z}\end{pmatrix},$$

where p_{p_y} and p_{p_z} are completely defined by the motion of the rigid body and can therefore be incorporated into the total momentum of the rigid body. The component p_{p_x}, on the other hand, is unconstrained in the longitudinal direction and thus represents an additional degree of freedom that should be explicitly accounted for. Besides, the definition of the momentum of the buoyancy control system can be incorporated into the total momentum of the rigid body.

The dynamic equations in the body frame are

$$\dot{\boldsymbol{p}}=\boldsymbol{p}\times\boldsymbol{\omega}+W\boldsymbol{\zeta}+\boldsymbol{f}_{\mathrm{v}}, \tag{4}$$

$$\begin{aligned}\dot{\boldsymbol{h}}=&\boldsymbol{h}\times\boldsymbol{\omega}+\boldsymbol{p}\times\boldsymbol{v}+m_{\mathrm{rb}}g\boldsymbol{r}_{\mathrm{rb}}\times\boldsymbol{\zeta}\\&+m_{\mathrm{b}}g\boldsymbol{r}_{\mathrm{b}}\times\boldsymbol{\zeta}+m_{\mathrm{p}}g\boldsymbol{r}_{\mathrm{p}}\times\boldsymbol{\zeta}+\boldsymbol{m}_{\mathrm{v}},\end{aligned} \tag{5}$$

$$\dot{p}_{p_x}=\boldsymbol{e}_1\cdot(\boldsymbol{p}_{\mathrm{p}}\times\boldsymbol{\omega}+m_{\mathrm{p}}g\boldsymbol{\zeta})+u_{p_x}, \tag{6}$$

where $\boldsymbol{\zeta}=\boldsymbol{R}_{\mathrm{IB}}^{\mathrm{T}}\boldsymbol{i}_3$ is the 'tilt vector', the body frame unit vector in the direction of gravity, and u_{p_x} is input force from the actuator which adjusts the glider attitude.

The terms $\boldsymbol{f}_{\mathrm{v}}$ and $\boldsymbol{m}_{\mathrm{v}}$ represent viscous effects acting on the glider expressed in the body frame. These forces and moments include viscous forces (such as lift and drag) and control moments (such as the yaw moment due to a rudder). The hydrodynamic forces and moments above are expressed in the 'current' reference frame. Let α=arctan(w/u) denote the vehicle's 'angle of attack' and let β=arsin(v/||$\boldsymbol{v}$||) denote the 'sideslip angle'. The current frame is related to the body frame through a proper rotation matrix

$$\boldsymbol{R}_{\mathrm{BC}}(\alpha,\beta)=\mathrm{e}^{-\hat{\boldsymbol{e}}_2\alpha}\mathrm{e}^{\hat{\boldsymbol{e}}_3\beta}.$$

See Etkin and Reid (1995), for example. Following the standard modeling conventions (McCormick, 1979; Etkin and Reid, 1995), we write

$$\boldsymbol{f}_{\mathrm{v}}=-\boldsymbol{R}_{\mathrm{BC}}\begin{pmatrix}D(\alpha)\\ S_\beta\beta+S_{\delta_{\mathrm{r}}}\delta_{\mathrm{r}}\\ L_\alpha\alpha\end{pmatrix},$$

$$\boldsymbol{m}_{\mathrm{v}}=\boldsymbol{D}_\omega\boldsymbol{\omega}+\begin{pmatrix}K_\beta\beta+K_{\delta_{\mathrm{r}}}\delta_{\mathrm{r}}\\ M_\alpha\alpha\\ N_\beta\beta+N_{\delta_{\mathrm{r}}}\delta_{\mathrm{r}}\end{pmatrix}.$$

The various coefficients, such as L_α and N_β, depend on the vehicle speed, through the dynamic pressure, the geometry, and the Reynolds number. The matrix $\boldsymbol{D}_\omega$ contains terms which characterize viscous angular damping (such as pitch and yaw damping) (Mahmoudian, 2009). $S_{\delta_{\mathrm{r}}}$, $K_{\delta_{\mathrm{r}}}$, and $N_{\delta_{\mathrm{r}}}$ represent the sideslip force, roll, and yaw moment coefficients due to a rudder, respectively.

According to Eqs. (4)–(6), along with the buoyancy actuator dynamics, the glider dynamics is described as

$$\dot{\tilde{V}}_{\mathrm{b}}=u_{\mathrm{b}}, \tag{7}$$

where u_{b} is the input force from the actuator, which adjusts the net weight of the glider. Together with the kinematic Eqs. (1)–(3), these equations completely describe the motion of the vehicle in still water.

3 Dynamic model analysis

Based on the derived dynamic model, steady flight equilibrium analysis and stability analysis are carried out in this section. Steady flight equilibrium analysis is important for motion control and path planning, as well as for vehicle design, as it may provide guidelines for sizing actuators and stabilizers. Stability analysis is used to provide guidelines for vehicle geometry design. Similar to aircraft study, glider geometric parameters determine the hydrodynamic coefficients, which will further affect the stability of glider motion (Fan *et al.*, 2012).

3.1 Steady flight equilibrium

The purpose of this analysis is to obtain the basic design parameters for glider development, including the varied range of moving mass location ($\bar{r}_{p_x}$) for pitch angle control and the varied range of the volume of the ballast system ($\bar{V}_\mathrm{b}$) for buoyancy control. The steady-state flight conditions are determined by solving the nonlinear state Eqs. (4) and (5) for the state and control vectors that make the state derivatives identically zero:

$$\dot{\boldsymbol{p}} = \boldsymbol{0}\,,\ \dot{\boldsymbol{h}} = \boldsymbol{0}\,.$$

Because of the complexity involved in computing an analytical solution, numerical algorithms for computing 'trim conditions' are necessary. A numerical trim solver is developed based on Matlab's fsolve subroutine, with which we can obtain the steady flight equilibrium much more easily and accurately than an analytical solution, as in Mahmoudian *et al.* (2010). This trim solver can also serve to determine the feedforward terms of the feedforward/feedback controller for glider motion control (Mahmoudian and Woolsey, 2008).

The numerical trim solver takes the desired steady motion parameters (speed, pitch angle, or heading angle) and determines the required inputs for actuation (the moving mass and rudder location, and the varied volume of the ballast system). In applications where inertial velocity measurements are available, it may be more appropriate to regulate the glide path angle and course angle rather than the pitch angle and heading angle. However, inertial velocity measurements are typically unavailable for an underwater glider. For most of the time the glider moves in the wings-level flight condition steadily and efficiently. Here we take glider wings-level steady flight as an example to introduce our numerical equilibrium-finding results. Some of the physical and hydrodynamic characteristics used in the numerical calculation are initially referred to a model of Slocum presented in earlier studies (Graver, 2005; Bhatta, 2006).

For our case, the masses of the pitch control module (m_p) and the buoyancy control module (m_b) are 10 and 5 kg, respectively, and their locations are initially set at 0.25 m fore and 0.5 m aft of the center of vehicle buoyancy, respectively. The mass of the glider rigid body (m_rb) is 45 kg, whose center of mass is located 0.05 m under the center of vehicle buoyancy vertically. Tables 1 and 2 show two sets of wings-level equilibriums during glider descending in order to determine the design parameters $\bar{r}_{p_x}$ and $\bar{V}_\mathrm{b}$. Table 1 shows that, for the same gliding speed V= 0.4 m/s, when the pitch angle θ changes from −5° to −60°, the location of the moving mass r_{p_x} changes from 272.0 to 640.1 mm and the amount of volume variation $\tilde{V}_\mathrm{b}$ changes from −215.9 to −37.5 ml. Table 2 shows that, for the same pitch angle θ=−35°, which is the maximum horizontal velocity flight condition of glider motion (Graver, 2005), when the gliding speed V changes from 0.1 to 0.8 m/s, the required amount of volume variation $\tilde{V}_\mathrm{b}$ changes from −3.5 to −223.1 ml, while the location of the moving mass r_{p_x} does not change too much, from 407.6 to 410.0 mm. While wings-level equilibriums are symmetrical for

Table 1 Wings-level equilibriums with a fixed gliding velocity (V=0.4 m/s)

θ (°)	r_{p_x} (mm)	α (°)	$\tilde{V}_\mathrm{b}$ (ml)
−5	272.0	5.52	−215.9
−10	291.3	3.80	−150.3
−15	311.5	2.78	−112.5
−20	332.9	2.15	−89.2
−25	355.7	1.72	−74.0
−30	380.6	1.41	−63.4
−35	408.2	1.17	−55.8
−40	439.3	0.99	−50.1
−45	475.5	0.83	−45.7
−50	518.6	0.70	−42.3
−55	571.8	0.58	−39.6
−60	640.1	0.48	−37.5

glider descent and ascent motions, based on numerical calculation of wings-level descent equilibrium, we choose $\bar{r}_{p_x} = \pm 300$ mm and $\bar{V}_b = \pm 250$ ml as our design parameters for glider development; thus, we can obtain the maximum pitch angle 50° and the maximum gliding speed 0.8 m/s at least. Since then, the length of the glider sealed hull is initially identified as 1.5 m.

Table 2 Wings-level equilibriums with a fixed pitch angle (θ=−35°)

V (m/s)	r_{p_x} (mm)	α (°)	$\tilde{V}_b$ (ml)
0.1	407.6	1.17	−3.5
0.2	407.7	1.17	−13.9
0.3	407.9	1.17	−31.4
0.4	408.2	1.17	−55.8
0.5	408.5	1.17	−87.2
0.6	408.9	1.17	−125.5
0.7	409.4	1.17	−170.8
0.8	410.0	1.17	−223.1

3.2 Stability analysis

Here, a stability analysis is made to discuss the relationship between the stability of glider motion and the location of glider wings and rudder, by viewing glider dynamics as a multi-degree-of-freedom eigenvalue problem using linear algebra solution techniques. To achieve this, considering a glider with fixed actuators as a rigid body, we linearize the dynamic equations about a wings-level equilibrium condition. Fixed actuators mean that the actuator parameters, such as a moving particle, vehicle buoyancy, and rudder deflection angle, are assumed to remain constant. In aircraft stability and control theory, such an analysis is referred to as 'stick-fixed' stability analysis, since it is assumed that the pilot holds the 'stick' such that the control surfaces remain fixed in place (Etkin and Reid, 1995).

Based on the discussion in Section 3.1, we choose a set of descent equilibrium conditions in Table 2, which is V_{eq}=0.4 m/s, $\tilde{V}_{b\_eq} = -55.8$ ml, γ_{eq}=−35°, $r_{p_x\_eq} = 0.4082$ m, $\alpha_{eq} = 1.17$°. Linearizing the coupled and nonlinear dynamic equations about the above wings-level equilibrium, one finds that the resulting equations are decomposed into longitudinal- and lateral-directional components, each of which is a set of four, first-order, coupled ordinary differential equations (ODEs) with constant coefficients. Ignoring certain kinematic variables, one obtains two sets of equations in linear algebra form:

$$\dot{\boldsymbol{X}}_{\text{long}} = \boldsymbol{A}_{\text{long}}\boldsymbol{X}_{\text{long}} + \boldsymbol{B}_{\text{long}}\boldsymbol{u}_{\text{long}},$$

$$\dot{\boldsymbol{X}}_{\text{lat}} = \boldsymbol{A}_{\text{lat}}\boldsymbol{X}_{\text{lat}} + \boldsymbol{B}_{\text{lat}}\boldsymbol{u}_{\text{lat}},$$

where the longitudinal- and lateral-directional state vectors are

$$\boldsymbol{X}_{\text{long}} = [u, w, q, \theta]^{\text{T}},\ \boldsymbol{X}_{\text{lat}} = [v, p, r, \varphi]^{\text{T}}.$$

Next, we investigate the effect of a few critical geometric parameters on the eigenvalue distribution of the linearized dynamic model, in the chosen wings-level flight condition with all the actuators fixed. We present root locus plots for the longitudinal modes in terms of wing location l_w (the aerodynamic center of the wing is a distance l_w aft of the center of buoyancy), and for the lateral-directional modes in terms of rudder location l_r (the aerodynamic center of the rudder is a distance l_r aft of the center of buoyancy). Fig. 2 describes the definition of geometric parameters l_w and l_r.

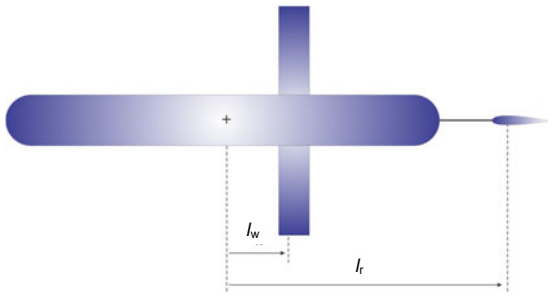

Fig. 2 Glider geometric parameters for stability analysis

Fig. 3 shows a root locus plot for the longitudinal modes in wings-level flight under the chosen equilibrium flight condition in terms of parameter l_w. In this plot, l_w varies from zero, in which case the wing is aligned with the center of buoyancy, to 0.2l (l is the length of the glider sealed hull). Note that the farther aft the wing is located, the more stable the glider longitudinal dynamics becomes, due in part to the increased pitch damping. This increased stability is beneficial to glider steady motion, but may also limit pitch control authority because of the increased arm of hydrodynamic force applied on the wings, a

tradeoff that should be considered for the layout of wings. Fig. 4 shows a root locus plot for the lateral-directional modes in the chosen equilibrium flight condition in terms of parameter l_r. In the plot, l_r varies from $0.5l$ to l, that is, from the stern end of the hull to a half vehicle length aft of the stern. The farther aft the rudder is located, the more stable the glider lateral-directional dynamics becomes, due to increasing yaw stiffness and damping. Again, there is another tradeoff between stability and control authority for the layout of the rudder.

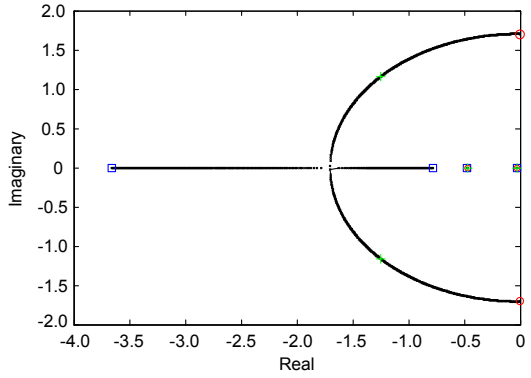

Fig. 3 Root locus plot for longitudinal modes with l_w
Root locus branches begin at circles and end at squares. The crosses represent the eigenvalues of glider longitudinal dynamics with chosen design parameters

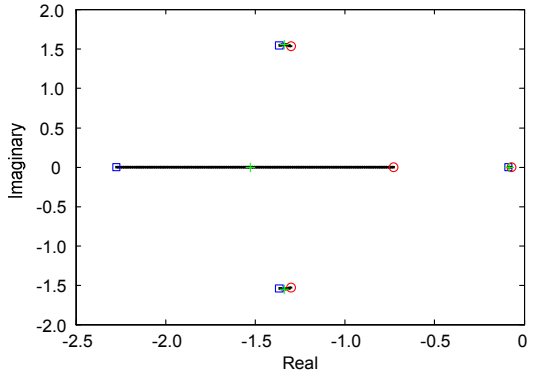

Fig. 4 Root loci plots for lateral-directional modes with l_r
Root locus branches begin at circles and end at squares. The crosses represent the eigenvalues of glider lateral-directional dynamics with chosen design parameters

The increased stability may provide better response to disturbances, but meanwhile it may limit the control authority of glider motion. Tradeoffs between control authority and stability are fundamental in vehicle design and they suggest the need for stability requirements or guidelines. For manned vehicles, such guidelines are obtained based on crew and passenger comfort. For unmanned vehicles, a primary concern may be motion of the payload in response to disturbances. In any case, the tradeoff can be addressed based on a clear statement of mission requirements (Fan *et al.*, 2012).

For our case, the wings and rudder are designed with a swept-back angle, not only to increase glider motion stability in pitch and yaw (Warren, 2009), but also to reduce weed accumulation (Webb *et al.*, 2001). Balancing the requirements of stability and control authority of glider mission, for the equivalent rectangular wing and rudder (Mason, 2001), we choose l_w=0.15l and l_r=0.8l as our design parameters. The longitudinal- and lateral-directional stability of glider dynamics with the chosen design parameters is marked by crosses in Figs. 3 and 4. In our case, the stability of the glider may provide a better response to disturbances and the control authority is attainable.

4 Glider prototype development

With the key glider design parameters determined by dynamic model analysis, we aim to develop a coastal underwater glider serving as an ocean observatory platform in the East China Sea. As the depth of the East China Sea is mostly less than 200 m (Encyclopedia Britannica, 2012), our glider is designed to operate in 200 m deep water.

4.1 Specifications and design scheme

Referring to the features of the underwater glider discussed in Rudnick *et al.* (2004), our glider is composed of a hull with wings, an attitude control system for pitch and turning control, a buoyancy control system, electrical hardware (e.g., controller, communication terminals, navigation and positioning devices, sensors, and batteries), and PC interface software. Some key specifications of the glider are listed in Table 3.

According to glider functional requirements, the whole glider system is organized into three layers: organization layer, coordination layer, and execution layer. The flowchart of the glider system is presented in Fig. 5. The organization layer is responsible for mission planning, control command downloading, sample data processing, and vehicle running status monitoring. The coordination controller dominates

Table 3 Key glider specifications

Parameter	Value
Body length	1.5 m
Full body (with rudder)	2.1 m
Diameter	220 mm
Mass	60 kg
Buoyancy engine displacement	0–500 ml
Endurance	20 d
Depth	200 m
Pitch control authority	±50°
Deflection angle of rudder	±60°

the whole coordination layer and coordinates all the equipment in the vehicle (including communication terminal, navigation and positioning devices, data logger, a variety of sensors, and so on), making them work orderly and effectively. The controller communicates with the organization layer receiving control commands and sending running status, motion state, and sample data. The actuators for attitude control and buoyancy control belong to the execution layer, and the communication between the coordination layer and the execution layer is via a controller area network (CAN) bus to obtain real-time motion control.

4.2 ZJU glider configuration

To modularize the vehicle and for easy system assembly, our glider is designed with modular architecture. The sealed cylinder hull is divided into three parts: pitch control system bay (front), electrical hardware bay (middle), and buoyancy control & turning control systems bay (rear). Besides, the communication and positioning terminals are sealed in the plastic rudder due to their functional requirements. Modular architecture allows other functional bays to be integrated into the existing platform easily extending the functionality of the vehicle, such as developing a wave-energy collecting unit to capture environmental energy, or adding additional propeller and control surfaces to increase the maneuverability of the glider. Water can pass through the front and rear elliptical hemispheres, which contain sensors and a bladder, respectively. Fig. 6 shows the configuration of the ZJU glider.

4.3 Functional modules

Next, we will present the main functional modules of our glider including the hull, buoyancy control

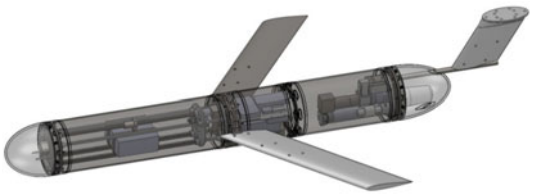

Fig. 6 ZJU glider configuration

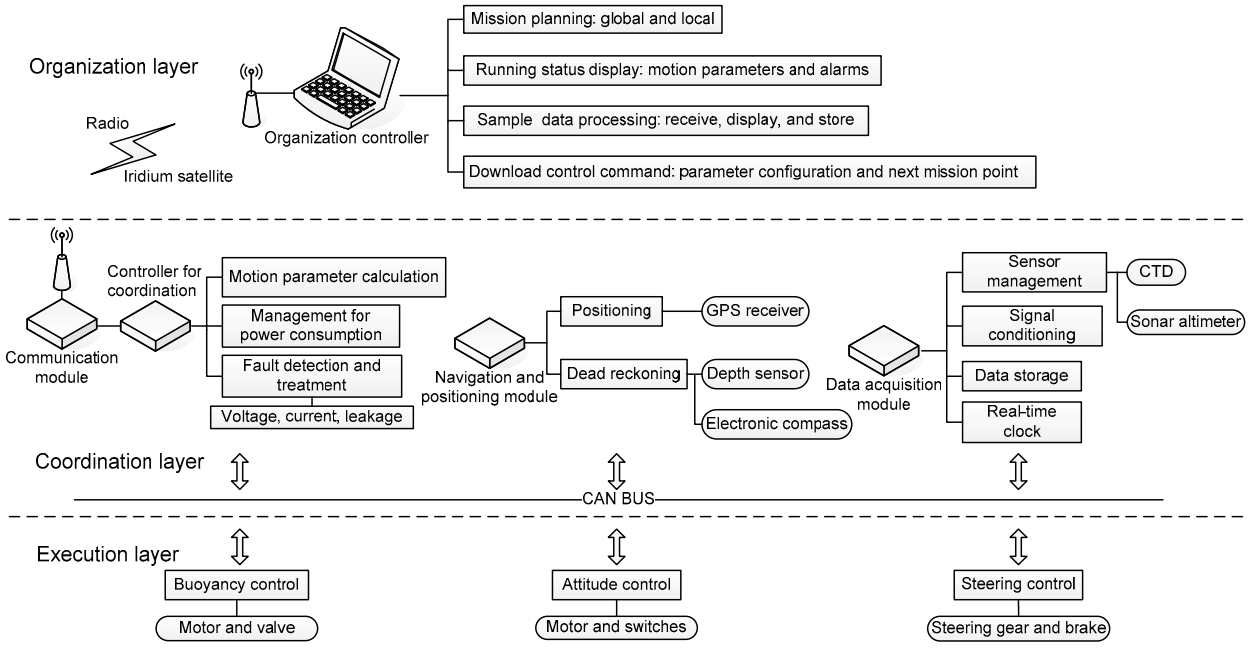

Fig. 5 Flowchart of the glider system

system, attitude control system, electrical hardware, and PC interface software. Since the maximum operational depth of the underwater glider is determined by the strength and sealing capability of the hull as well as the performance of the buoyancy control system, here we will introduce these two key modules in more detail.

4.3.1 Structural design

As the vehicle operates within 200 m deep water, the hull should withstand 2 MPa water pressure. The hull is also designed to have less mass and larger containing space to store more components and devices. For structural analysis, it is assumed that the main hull is a cylindrical tube with constant wall thickness. The hull is sized based upon yield and buckling criteria (Wang and Cai, 2005). Conventional structural analysis methods are used to size the wall thickness of the hull with a given length, in terms of a factor of safety of two or greater.

Referring to the sizes of the existing gliders (Eriksen *et al.*, 2001; Sherman *et al.*, 2001; Webb *et al.*, 2001), and also according to our needs, the entire length and inner diameter of the hull are chosen to be 1.5 m and 0.21 m, respectively. As our glider is designed with modular architecture, the glider hull is divided into three parts. The longest part of the hull is used to contain a pitch attitude control system. Based on the analysis in Section 3.1, the length of this part of the hull is chosen to be 0.75 m. Here, we just need to size the wall thickness using yield and buckling criteria with respect to this part of the hull. Considering that the end of each part of the hull is reinforced with rib structure, which will improve the mechanical strength of the hull a lot, we can select a smaller factor of safety during our calculation. The wall thickness of the hull is calculated with comparison among three different kinds of materials—stainless steel, hard aluminum alloy, and titanium alloy, which are commonly used for hull fabrication of underwater vehicles.

Depending on the yield criteria, the thickness of the hull δ is determined by

$$\delta_y \geq \frac{P_{max} D_i}{2[\sigma]\varphi_s - P_{max}} + C, \tag{8}$$

where P_{max} is the maximum working pressure, D_i is the inner diameter of the hull, $[\sigma]$ is the permissible stress, C is the additional value of wall thickness, φ_s is the weld joint efficiency, and δ_y is the wall thickness of strength check.

Since the glider hull is characterized as a thin-walled short cylinder (Wang and Cai, 2005), the buckling wall thickness check a necessary. Here, both the circumferential and axial buckling check is considered. The wall thickness of circumferential buckling criteria is obtained by

$$\delta_{bc} \geq D_o \left(\frac{m_c P_{max} L}{2.59 E D_o} \right)^{0.4}, \tag{9}$$

where D_o is the outer diameter of the hull, m_c is the factor of safety for circumferential stability (we choose m_c as 2 here), L is the length of the checked hull, E is the elastic modulus of the material, and δ_{bc} is the wall thickness of circumferential buckling criteria.

The permissible critical stress of axial buckling can be calculated by

$$[\sigma]_{cr} = \frac{0.182 E \delta}{m_a R}, \tag{10}$$

where m_a is the factor of safety for axial stability (we choose m_a as 3 here), R is the radius of the intermediate surface of the hull, and $[\sigma]_{cr}$ is the permissible critical stress of axial buckling.

Both the yield and buckling criteria are considered for each kind of material. Table 4 gives the characteristics and wall thickness calculation results of the three kinds of materials. The results indicate that the permissible critical stresses of axial buckling of all three materials are much greater than the maximum working pressure, so the size of wall thickness is determined by circumferential buckling criteria. Taking multiple factors into consideration, such as wall thickness, mass, corrosion resistance capability, and machining available, we choose titanium alloy as our hull material; the wall thickness of the hull is 4.2 mm. The performance of the hull we designed will be validated by pressure tests in Section 5.1.

4.3.2 Buoyancy control system

The variation of glider buoyancy is designed with an oil-filled bladder, which is inflated and deflated using a reciprocating pump to transfer oil between the

Table 4 Characteristics and calculation results of three different kinds of materials

Parameter	Value/Description		
	Stainless steel	Hard aluminum alloy	Titanium alloy
Composition	12Gr1MoV	LY12	TC4
Yield stress (MPa)	290	274	824
Permissible yield stress (MPa)	145	137	412
Tensile stress (MPa)	500	421	895
Permissible tensile stress (MPa)	167	143.3	298.3
Permissible stress (MPa)	145	137	298.3
Wall thickness of strength check (mm)	1.5	1.6	0.8
Elastic modulus (MPa)	2×10^5	6.2×10^4	1.06×10^5
Wall thickness of circumferential buckling criteria (mm)	3.24	5.18	4.15
Permissible critical stress of axial buckling (MPa)	369.54	182.11	255.04
Density (kg/m^3)	7900	2700	4500
Mass of the hull (kg)	29.5	15.1	20.5
Corrosion resistance capability	Not good	Good	Better

reservoir inside the vehicle hull and an external bladder exposed to the water. A solenoid valve is used to shut off the oil channel when needed. As a common disadvantage of the micro reciprocating pump is oil leakage, especially under high pressure, here we adopt an open-formed reciprocating pump, which is immersed into a sealed oil cylinder, and use dynamic sealing to seal the shaft of the pump. This method solves the leakage problem effectively. The reservoir is designed as the hydraulic cylinder form, and we use a pull-wire displacement sensor to measure the displacement of the cylinder piston, with which the volume of inflated and deflated oil can be estimated correctly. To make the buoyancy control system compact and smart, we adopt a hydraulic valve plate to fix all the components of the buoyancy control system together. The mechanical structure of the buoyancy control system is shown in Fig. 7. Based on the theoretical analysis in Section 3.1, the maximum effective capacity of the cylinder and the bladder is designed to be a little more than 500 ml, to provide enough varied volume for buoyancy control. The chosen motor and pump are powerful enough to pump oil into the bladder outside, withstanding water pressure at 200 m depth.

The hydraulic simulation module of AMESim software is used to investigate the feasibility and dynamic performances of the buoyancy control system. An equivalent simulation model is developed according to our needs (Fig. 8a). Two cylinders are taken as the internal reservoir and the external bladder, respectively. A force applied to the piston rod of the reservoir cylinder acts as the friction force during

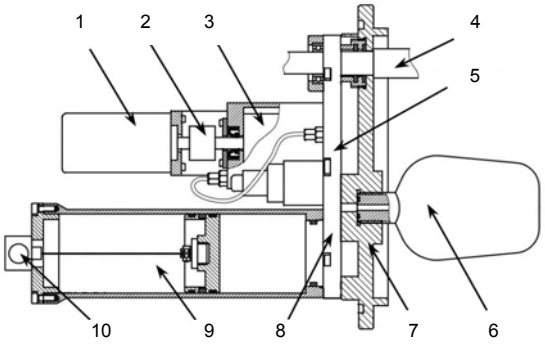

1. motor; 2. coupling; 3. reciprocating pump immersed in an oil cylinder; 4. rudder rod; 5. solenoid valve; 6. bladder; 7. endcap of glider hull; 8. valve plat; 9. oil cylinder; 10. pull-wire displacement sensor

Fig. 7 Mechanical structure of the buoyancy control system

piston motion; another force applied to the piston rod of the bladder cylinder simulates the pressure from seawater. A flow meter is used to measure the volume of inflated or deflated oil in our simulation; the measurements can be taken as feedback to switch the external force and control the action of the motor and the solenoid valve.

The varied range of bladder volume is 0–500 ml; the maximum load pressure is 2 MPa; the displacement of the pump is 1.1 ml/r; and the output speed of the actuator is 470 r/min. In fact, we obtain the volume of inflated or deflated oil from the measurement of the location of the reservoir cylinder piston. The diameter of the cylinder piston is 50 mm, and the piston stroke of the reservoir cylinder is 300 mm. The piston moves from 22.5 to 277.5 mm in the cylinder to deflate the bladder when the glider dives and

moves in the opposite direction to inflate the bladder when the glider rises (Fig. 8b). Simulation results indicate that the hydraulic system is feasible. Note that it takes about 57 s to inflate or deflate 500 ml of oil with the given operational parameters of hydraulic components. The actual performance of the buoyancy control system will be validated in Section 5.1.

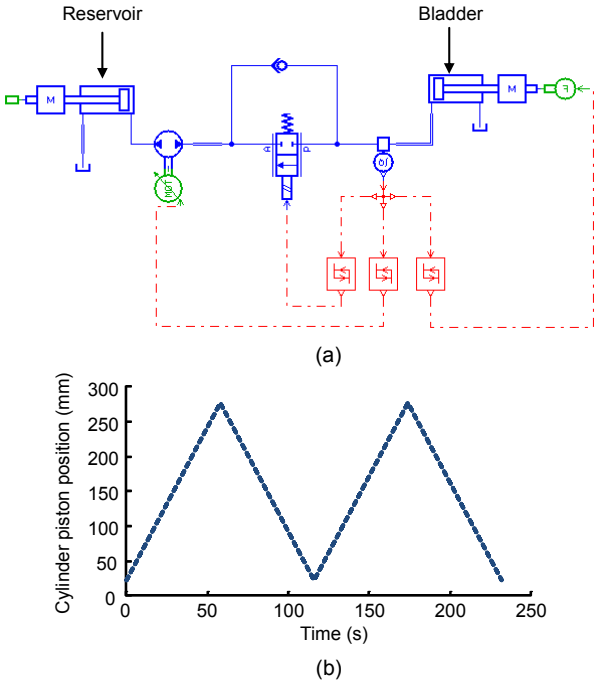

Fig. 8 AMESim simulation of the buoyancy control system
(a) AMESim model; (b) Simulation result

4.3.3 Attitude control system

The implementation of our pitch control system is based on a screw-nut assembly, and a battery package is fixed to the moving nut and taken as the moving mass. The moving range of the mass is designed according to the analysis in Section 3.1. The worm gear and worm are used to reduce the motor speed and increase the torque of the motor. Moreover, the self-locking capability of worm gear and worm is quite necessary for our requirement that the mass should be locked at a certain location when it stops. Besides, a pair of limit switches is used to ensure that the moving mass moves within the available range.

Here, we use a rudder to achieve a turning motion in order to have fast maneuverability in shallow water. A steering motor actuates the rudder rod to swing the rudder, and a dynamic rotating seal is used to seal the rudder rod. When the glider moves in the longitudinal plane and the turning motion is not needed, the rudder is locked by a normally closed electromagnetic brake. The mechanical structure of our glider attitude control system is presented in Fig. 9.

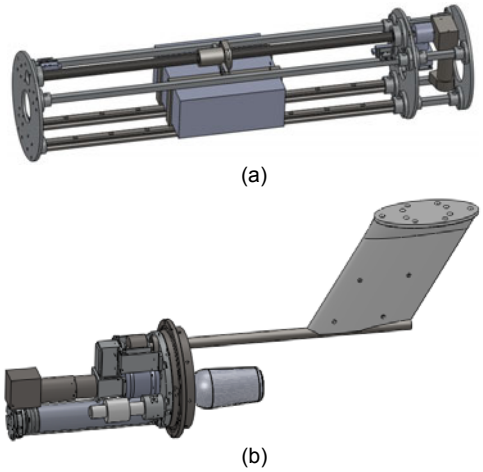

Fig. 9 Attitude control system
(a) Pitch control; (b) Turning control

4.3.4 Electrical hardware

The control system embedded in the vehicle is the core of glider electrical hardware. The glider control system is based on a TMS320F28335 (TI, USA) controller, which is expert in both accurate signal processing and real-time motion control. Its multiple peripheral ports are very convenient for the integration of other functional devices. Glider functional devices include an electronic compass (PNI TCM5), a GPS receiver (NovAtel OEMV-3), a communication terminal (Freewave FGR115RC/WC), and a CTD (Sea-Bird GPCTD). Two main functions of the control system are data acquisition (board 2) and motion control (board 3) (Fig. 10). Some necessary circuit modules are developed to expand the functionality of the system including serial port expansion, signal conditioning, external memory expansion, real-time clock, voltage regulation, as well as communication and switch isolation. A polymer lithium battery package whose power capacity is 45 A·h supplies energy for the operation of the whole glider system.

4.3.5 PC interface software

The PC interface software plays an important role in system operation, with which the interaction between the human organizer and the glider vehicle is

achieved through communication terminals. It possesses multiple functions, such as monitoring system running status, sending control commands, displaying glider motion state, as well as processing the sampled data including data receiving, display, and storage, when the glider dwells on the surface of the water. We adopt an error-detection mechanism during communication and provide data transmission with error-recovery ability, to guarantee accurate and reliable command/data sending and receiving accurately and reliably. The interface of PC software is shown in Fig. 11.

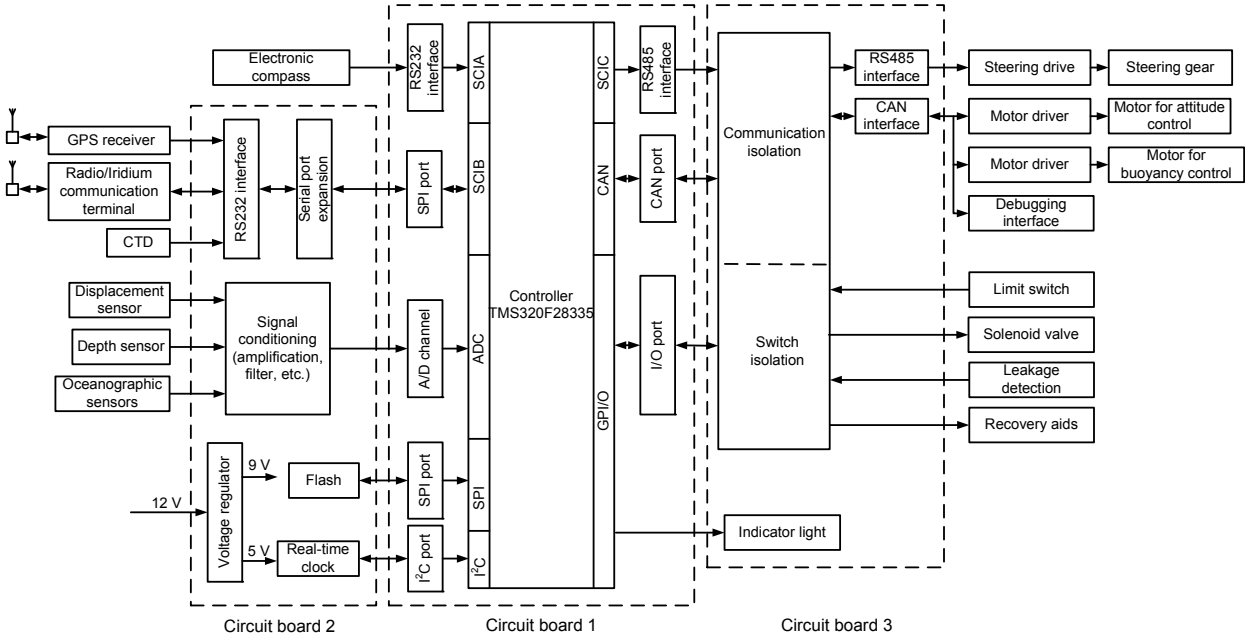

Fig. 10 Organization of glider electrical hardware

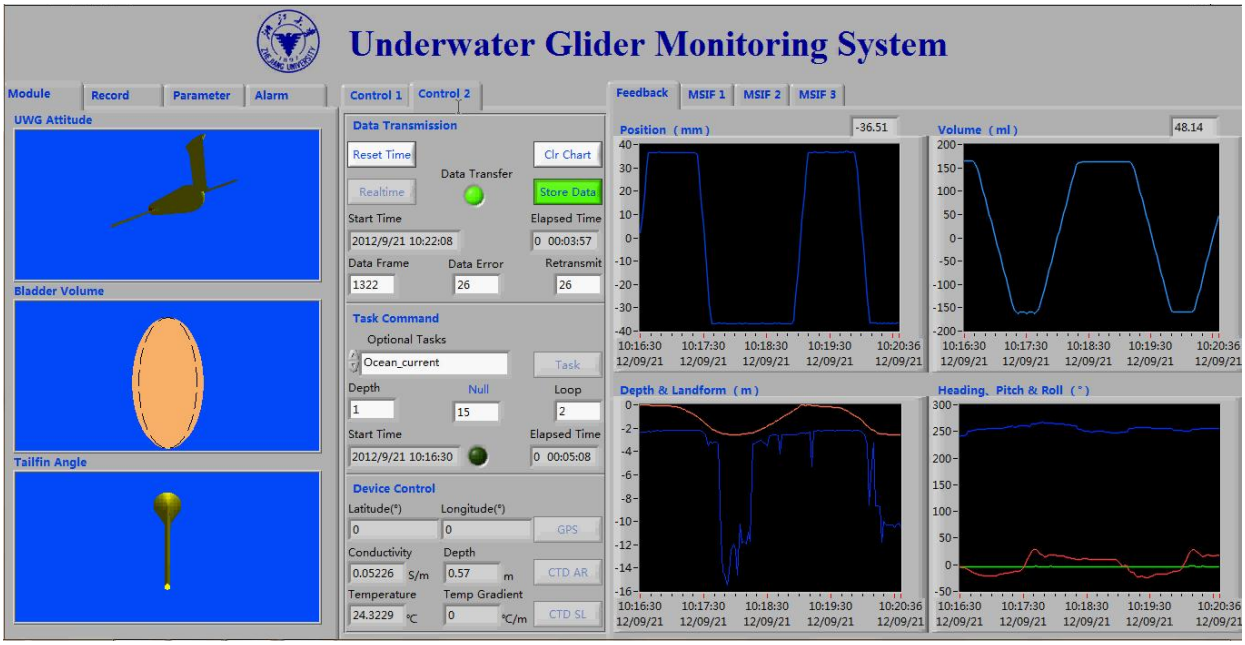

Fig. 11 PC interface software of the glider

5 Validation of the prototype

The validation of the prototype was carried out step by step. First, we tested and ensured the performance of glider key functional modules individually, which are the hull and the buoyancy control system. Then it might be feasible to assemble the whole system and validate the prototype with an in-water trial.

5.1 Functional modules test

5.1.1 Pressure tests of the hull

There is a 60 MPa hyperbaric chamber in our lab, which could be used to test the strength and sealability of the hull. The divided bays were assembled together with O-rings for static sealing (connection between different bays, endcaps, and bladder) and dynamic sealing (connection between rudder rod and endcap). The hull was put into the hyperbaric chamber, which is filled with water. By controlling a pump outside, the pressure inside the chamber can be increased up to certain pressure required (Fig. 12).

(a)

(b)

Fig. 12 Pressure test of the hull in the hyperbaric chamber
(a) Putting the hull into the hyperbaric chamber; (b) Reading from the pressure gauge

To simulate the pressure applied on the glider during its gliding motion, pressure tests of the hull were carried out intermittently for several cycles. For each cycle, the pressure was increased up to more than 2 MPa, held for a while and then decreased to 0 MPa. The pressure test cycles were recorded in Table 5. Note that for each pressure holding phrase, the pressure was successfully maintained at greater than 2 MPa. There appeared gradual reduction in pressure for each pressure test cycle (the amount of the reduced pressure is less than 0.1 MPa), which was due to a very gradual change in chamber volume and hull volume when the chamber and hull are under high pressure. According to our operation experience, this small amount of pressure reduction is acceptable. With careful checking, we found the hull was intact and the sealability of the hull was good after the hull was taken out of the chamber.

Table 5 Pressure test cycles

No.	Time (hh:mm)	Pressure (MPa)
1	From 16:45	2.360
	To 17:15	2.293
2	From 17:30	2.392
	To 18:30	2.317
3	From 18:45	2.390
	To 19:45	2.317
4	From 20:00	2.308
	To 20:30	2.266
5	From 20:45	2.418
	To 21:45	2.372
6	From 22:00	2.410
	To 23:00	2.385

5.1.2 Performance tests of the buoyancy control system

Although the hyperbaric chamber has a large adjusting range of pressure, the sensitivity of adjusting is bad. It is hard to accurately adjust the pressure to a certain value under 1 MPa; what is more, there exists a dead zone at the beginning of the adjusting. So, it is unavailable to use the 60 MPa hyperbaric chamber to carry out the pressure test of the buoyancy control system. We thought up a novel idea to have a better understanding of the performance of the buoyancy control system under different pressures (within 2.5 MPa). When the glider works in the water, only the hull and the bladder are exposed to water, and the other parts of the buoyancy control system are sealed inside the hull. Since then, we just need to design a small hyperbaric chamber which is large enough to

contain the bladder. The bladder withstands the pressure inside the chamber, while the other parts of the buoyancy control system are exposed to the air. Similar to the operation of the large hyperbaric chamber, we used a manual pump to slowly fill the small hyperbaric chamber with water; thus, the rate of pressure increase could be under accurate control (Fig. 13).

As the performance of the motor and pump is not only based on their individual qualities, but also affected by the operating parameters that properly match each other and the load effect. During our tests, we tried to investigate the efficiency of the motor and pump system with different speeds under different pressures in order to obtain the optimal speed. The efficiency could be described as follows:

$$\eta=\frac{W_{\text{useful}}}{W_{\text{total}}}=\frac{PSl_{\text{piston}}}{UIt}=\frac{PS}{K},\quad K=\frac{UIt}{l_{\text{piston}}},$$

where η is the efficiency of the motor and pump system, W_{useful} is the useful work done by the motor and pump system, W_{total} is the total work done by the motor and pump system, P is the pressure load caused by seawater, S is the cross-sectional area of the cylinder piston, U is the operating voltage of the motor, I is the operating current of the motor, t is the work time of the motor and pump system, l_{piston} is the displacement of the cylinder piston, and K denotes the amount of power consumption when driving the reservoir cylinder piston moving per millimeter of displacement. It is clear that if P and S are constant, η is inversely proportional to K. Besides, we investigated the response performance of the buoyancy control system at the optimal speed under different pressures.

We chose the Maxon EC 45 motor (the input voltage is 24 V) as our actuator for buoyancy control. The motor is equipped with a reducer, whose reduction is 15:1, to increase the driving torque of motor and

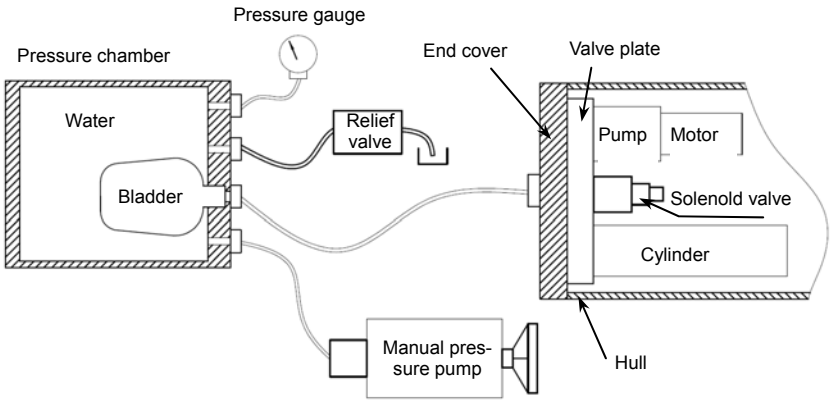

(a)

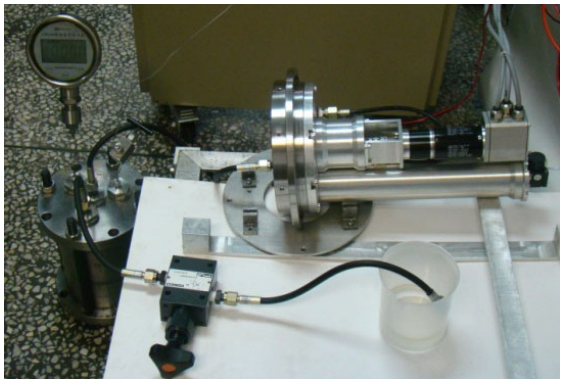

(b)

Fig. 13 Pressure test of the buoyancy control system in a small hyperbaric chamber: (a) schematic of pressure test; (b) picture shot from pressure test

decrease the speed of motor. The rated ratio decrease motor speed. The rated displacement of the reciprocating pump is 1.1 ml/r. Because of the transmission losses and the load effect, the efficiency of the motor and pump will change. During our tests, the efficiency of the motor and pump was first investigated under different pressures, from 0 to 2.5 MPa, with 0.5 MPa as the interval. For each pressure, the speed of the motor varied from 3500 to 8750 r/min, with 1750 r/min as the interval (Fig. 14). The designed test was aimed to find the optimal speed, at which the lowest power consumption could be obtained, as well as the acceptable rate of oil inflating or deflating. Based on the test results, we chose 7000 r/min as our motor speed. System response under different pressures with motor working at 7000 r/min is presented in Fig. 15. Note that as the pressure increases, more time is needed to propel the piston of the reservoir cylinder moving the same length of distance; this means it is harder to inflate the same volume of oil when the glider ascends at a deeper depth. The system response of test at 0 MPa is similar to the simulation results in Section 4.3.2. It took around 60 s to inflate 500 ml of oil for both the test (under 0 MPa) and the simulation (under 2 MPa), but about 20 s more to inflate the same volume of oil at 2 MPa during tests. It is because all

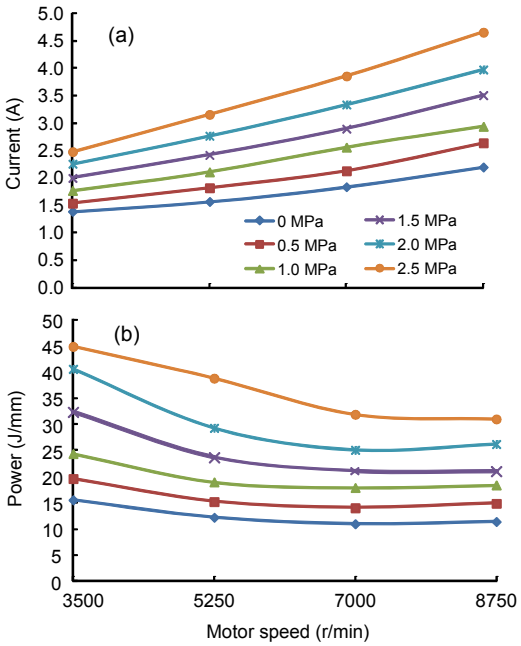

Fig. 14 Motor performance at different speeds, under different pressures: (a) average current; (b) power consumption when driving the reservoir cylinder piston moving per millimeter of displacement

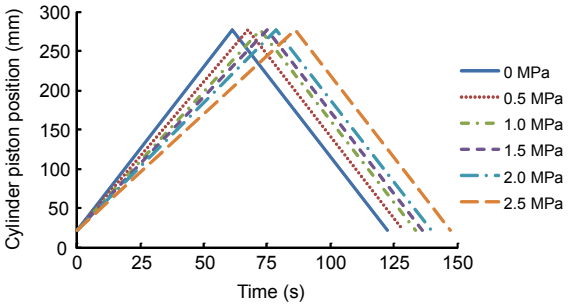

Fig. 15 System response under different pressures with motor working at 7000 r/min

the hydraulic components work under ideal conditions in simulation, and the transmission losses and load effect are not considered.

5.2 Pool trials

The glider prototype pool trials involved the work on mechanical components assembly, electrical hardware integration, and the whole system debugging based on software. After system trimming, glider trials in the pool were carried out. Limited by the depth of the pool (3.5 m), preliminary trial results of glider working were obtained. The pool trials aimed to (1) detect the cooperating ability of glider motion modules for attitude control and buoyancy control, (2) test the coordination capability of the controller embedded in the vehicle and the performance of various electronic devices, such as communication terminals, navigation and positioning devices and sensors for sampling, and (3) examine the multiple functions of PC interface software.

The glider followed an up-and-down, sawtooth-like profile through the water. Its descent and ascent motion was captured by an underwater camera fixed in the pool; the pictures shot by the camera are shown in Fig. 16. The vehicle communicated with an onshore control computer periodically when it appeared on the surface of the water via radio. The plots in Fig. 17 present glider motion data recorded by PC interface software, including the varied volume of bladder, glider attitude, and glider path. It seemed that the electronic compass for attitude measurement gave a faulty heading reading. There existed a range of 35° drift, which should not happen during glider motion in the longitudinal plane. Actually, the accuracy of the compass for heading measurement is 0.3°, so we inferred that the unexpected drift might be due to the disturbance from other magnetic devices, such as the

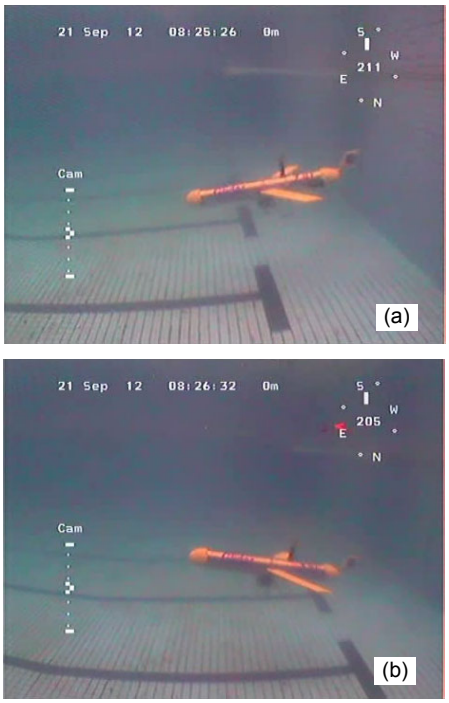

Fig. 16 Glider trial in the pool: (a) glider descending; (b) glider ascending

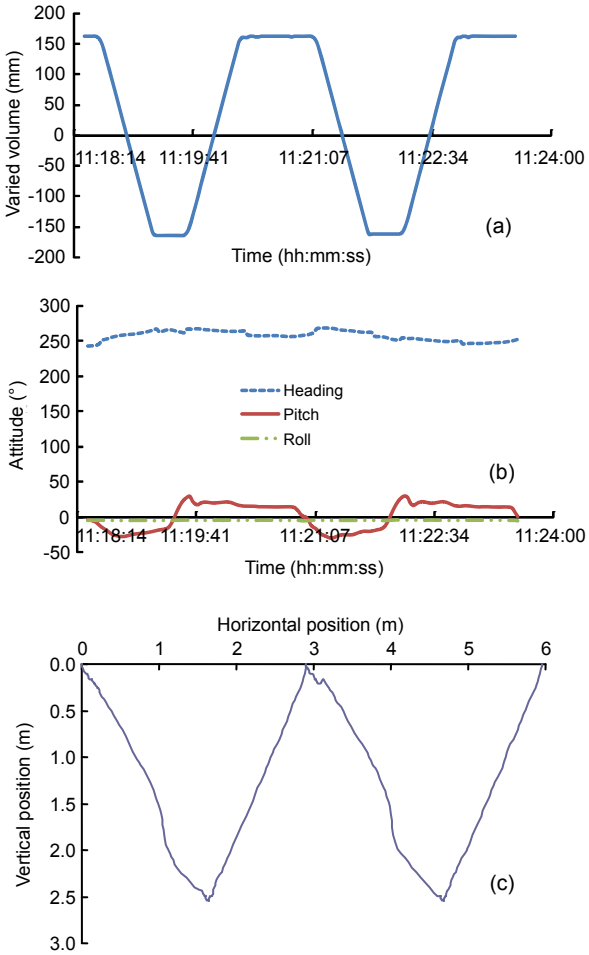

Fig. 17 Measurements of glider motion during pool trials: (a) varied volume of the bladder; (b) glider attitude; (c) glider path

motors and solenoid valve. Improvement in the solution is underway by shielding treatment of the disturbing magnetic devices. Pool trials indicated that most modules of our glider functioned well in water and the glider was capable of serving as a sensor platform for ocean sampling with some necessary improvements. Next, more trials will be carried out in deep water to have a better understanding of glider operating characteristics.

6 Conclusions

The ZJU glider was developed based on dynamic model analysis. Theoretical analysis served as design tools providing key design parameters for underwater glider development. Steady flight equilibrium analysis gave the varied range of moving mass location for pitch control and the varied vehicle volume for buoyancy control; a stability analysis was made to discuss the relationship between the stability of glider motion and the location of glider wings and rudder by root locus investigation of glider longitudinal- and lateral-directional dynamics, respectively. There is a tradeoff between glider motion stability and control authority according to the specific glider mission requirements. Based on theoretical analysis, the development of the ZJU glider was carried out. The prototype is composed of several functional modules including mechanical structure, a buoyancy control module, an attitude control module, electrical hardware, and PC interface software. Conventional structural calculation was used to determine the size and material of mechanical structure, and the strength of the chosen mechanical structure was validated by pressure test in the hyperbaric chamber. The feasibility of the buoyancy control module was first checked by AMESim simulation, and the performance of this module was validated by a special type of pressure test we designed, with which the most efficient motor speed for actuation was obtained. Besides, the response performance of the buoyancy control system at this speed was investigated. Lastly, preliminary

pool trials of the ZJU glider were introduced, and the prototype worked well during the pool trials. Glider trials in deeper water will be carried out next to make sure that the vehicle can be finally deployed in the East China Sea serving as an ocean observatory platform. Our ongoing research is focused on developing an effective algorithm for glider motion control and path planning, especially under the effect of unsteady or non-uniform currents.

Acknowledgements

The first author gratefully acknowledges the kind and patient academic guidance of Prof. Graig A. WOOLSEY during her visit at Virginia Tech.

References

Bhatta, P., 2006. Nonlinear Stability and Control of Gliding Vehicles. PhD Thesis, Princeton University, New Jersey, USA.

Encyclopedia Britannica, 2012. Encyclopædia Britannica Online Academic Edition. Encyclopædia Britannica Inc. Available from http://global.britannica.com/EBchecked/topic/176576/East-China-Sea [Accessed on Dec. 15, 2012].

Eriksen, C.C., Osse, T.J., Light, R.D., Wen, T., Lehman, T.W., Sabin, P.L., Ballard, J.W., Chiodi, A.M., 2001. Seaglider: a long-range autonomous underwater vehicle for oceanographic research. *IEEE J. Ocean. Eng.*, **26**(4):424-436. [doi:10.1109/48.972073]

Etkin, B., Reid, L.D., 1995. Dynamics of Flight: Stability and Control. John Wiley and Sons, Inc., New York, USA, p.93-196.

Fan, S., Wolek, A., Woolsey, C.A., 2012. Stability and Performance of Underwater Gliders. IEEE OCEANS, p.1-10. [doi:10.1109/OCEANS.2012.6404993]

Fossen, T., 1995. Guidance and Control of Ocean Vehicles. John Wiley and Sons, Inc., New York, USA, p.5-54.

Graver, J.G., 2005. Underwater Gliders: Dynamics, Control and Design. PhD Thesis, Princeton University, New Jersey, USA.

Hussain, N.A.A., Arshad, M.R., Mohd-Mokhtar, R., 2011. Underwater glider modelling and analysis for net buoyancy, depth and pitch angle control. *Ocean Eng.*, **38**(16):1782-1791. [doi:10.1016/j.oceaneng.2011.09.001]

Jenkins, S.A., Humphreys, D.E., Sherman, J., Osse, J., Jones, C., Leonard, N.E., Bachmayer, R., Graver, J., Clem, T., Carroll, P., *et al.*, 2003. Underwater Glider System Study. Technical Report No. 53, Scripps Institution of Oceanography, University of California, San Diego, CA.

Leonard, N.E., Graver, J.G., 2001. Model-based feedback control of autonomous underwater gliders. *IEEE J. Ocean. Eng.*, **26**(4):633-645. [doi:10.1109/48.972106]

Li, J., Song, B., Shao, C., 2008. Tracking control of autonomous underwater vehicles with internal moving mass. *Acta Autom. Sin.*, **34**(10):1319-1323. [doi:10.3724/SP.J.1004.2008.01319]

Mahmoudian, N., 2009. Efficient Motion Planning and Control for Underwater Gliders. PhD Thesis, Virginia Polytechnic Institute and State University, Virginia, USA.

Mahmoudian, N., Woolsey, C.A., 2008. Underwater Glider Motion Control. IEEE Conf. on Decision Control, p.552-557.

Mahmoudian, N., Geisbert, J., Woolsey, C.A., 2010. Approximate analytical turning conditions for underwater gliders and implications for path planning. *IEEE J. Ocean. Eng.*, **35**(1):131-143. [doi:10.1109/JOE.2009.2039655]

Mason, W.H., 2001. Citing Electronic Sources of Information. Virginia Tech. Available from http://www.dept.aoe.vt.edu/~mason/Mason_f/ConfigAero.html [Accessed on June 15, 2012].

McCormick, B.W., 1979. Aerodynamics, Aeronautics and Flight Mechanics. John Wiley and Sons, Inc., New York, USA, p.22-210.

Newman, J.N., 1977. Marine Hydrodynamics. MIT Press, Cambridge, MA, USA, p.102-152.

Rudnick, D.L., Davis, R.E., Eriksen, C.C., Fratantoni, D.M., Perry, M.J., 2004. Underwater glider for ocean research. *Mar. Technol. Soc. J.*, **38**(1):48-59.

Sherman, J., Davis, R.E., Owens, W.B., Valdes, J., 2001. The autonomous underwater glider spray. *IEEE J. Ocean. Eng.*, **26**(4):437-446. [doi:10.1109/48.972076]

Stommel, H., 1989. The Slocum mission. *Oceanography*, **2**(1):22-25. [doi:10.5670/oceanog.1989.26]

Wang, S., Sun, X., Wang, Y., Wu, J., Wang, X., 2011. Dynamic modeling and motion simulation for a winged hybrid-driven underwater glider. *China Ocean Eng.*, **25**(1):97-112. [doi:10.1007/s13344-011-0008-7]

Wang, Z., Cai, R., 2005. The Design of Chemical Pressure Vessel. Chemical Industry Press, Beijing, China, p.148-156 (in Chinese).

Warren, F.P., 2009. Mechanics of Flight. John Wiley and Sons, Inc., Hoboken, New Jersey, USA, p.377-597.

Webb, D.C., Simonetti, P.J., Jones, C.P., 2001. SLOCUM: an underwater glider propelled by environmental energy. *IEEE J. Ocean. Eng.*, **26**(4):447-452. [doi:10.1109/48.972077]

Woolsey, C.A., 2005. Reduced Hamiltonian dynamics for a rigid body/mass particle system. *J. Guid. Control Dynam.*, **28**(1):131-138. [doi:10.2514/1.5409]

Yang, H., Ma, J., 2010. Nonlinear control for autonomous underwater glider motion based on inverse system method. *J. Shanghai Jiaotong Univ. (Sci.)*, **15**(6):713-718. [doi:10.1007/s12204-010-1074-3]

Yu, J., Zhang, A., Jin, W., Chen, Q., Tian, Y., Liu, C., 2011. Development and experiments of the sea-wing underwater glider. *China Ocean Eng.*, **25**(4):721-736. [doi:10.1007/s13344-011-0058-x]